

Prediction of Room Temperature Electric Field Reversal of Magnetization in the Family of $A_4B_3O_9$ Layered Oxides

Urmimala Dey^{1,2}, Emma E. McCabe¹, Jorge Íñiguez-González^{2,3}, and Nicholas C. Bristowe^{1,*}

¹Centre for Materials Physics, Durham University, South Road, Durham DH1 3LE, United Kingdom

²Luxembourg Institute of Science and Technology (LIST), Avenue des Hauts-Fourneaux 5, L4362, Esch-sur-Alzette, Luxembourg

³Department of Physics and Materials Science, University of Luxembourg, 41 Rue du Brill, L4422, Belvaux, Luxembourg



(Received 21 May 2024; revised 4 February 2025; accepted 28 February 2025; published 1 April 2025)

The promise of a strong magnetoelectric coupling in a multiferroic material is not only of fundamental interest, but also forms the basis of next generation memory devices where the direction of magnetization can be reversed by an external electric field. Using group-theory led first-principles calculations, we have identified a hitherto unknown polar phase of the $A_4B_3O_9$ layered oxides, where the polar mode couples to the magnetic modes through a rare Γ -point magnetoelectric-multiferroic coupling scheme such that the net magnetization can be directly reversed by an electric field switching of the polar mode. Furthermore, in agreement with previous experimental observations, we predict room temperature magnetism in $A_4B_3O_9$ oxides that indicates the promising practical applications of these compounds in the next generation memory devices.

DOI: 10.1103/PhysRevLett.134.136801

Introduction—Magnetoelectric-multiferroic (ME-MF) materials with intrinsic cross-coupling between electrical and magnetic order parameters are promising for the next generation memory devices where an external electric field can switch the direction of magnetization leading to enhanced speed and reduced power consumption [1–6]. So far, despite intensive research efforts, only a handful of bulk materials with electric field switchable magnetization have been predicted and observed in experiments [6–11], and unfortunately none that order at room temperature (RT). Therefore, the search for ME-MF materials with RT electric field control of magnetization remains of utmost importance for realistic applications in memory devices [6,12].

Such control of magnetization can be achieved in a (single phase) antiferromagnetic (AFM) ME-MF material where weak ferromagnetism (wFM) arises due to canting of the collinear AFM spins via the Dzyaloshinskii-Moriya interaction (DMI) [13–15]. Depending on the crystal structure and underlying symmetries, electric polarization (\mathbf{P}) can couple to the net magnetization (\mathbf{M}) in these materials via different mechanisms [7,8,16]. The advantage of these type of strategies is that, since the couplings are at odd order (sometimes called “improper” couplings), switching \mathbf{P} can necessarily switch \mathbf{M} . Inspired by these

ME schemes, Senn and Bristowe have enumerated the possible ME-MF couplings in perovskites using a group-theoretical approach [17]. However, since AFM orderings in perovskite systems are always described by zone-boundary irreducible representations (irreps) of the parent space group, even the lowest-order ME-MF coupling schemes must involve a two-step process, each step contributing odd order energy terms in \mathbf{P} and \mathbf{M} separately with codependent order parameters [17], as shown in Fig. 1(a).

More generally, however, it should be possible to construct a simpler Γ -point scheme where \mathbf{P} and \mathbf{M} couple with a Γ -point AFM ordering mode in an “improper” manner such that the crystal momenta, inversion symmetry, and the time reversal symmetry are preserved [see Figs. 1(b) and 1(c)]. When \mathbf{P} and AFM ordering modes couple to give rise to a net \mathbf{M} induced by the DMI, application of an electric field can directly reverse \mathbf{M} via the reversal of \mathbf{P} , since the primary AFM order parameter is less likely to switch due to magnetic anisotropy [2,7,18]. This simpler Γ -point ME-MF scheme, shown in Fig. 1(b), allows for the switching mechanism to be contained in only one trilinear term but likely requires proper ferroelectricity and has rarely been observed [7,19] to the best of our knowledge. On the other hand, the same Γ -point coupling in Fig. 1(c) can also explain the induction of improper ferroelectricity observed in some type-II MFs [20,21] where the AFM mode couples with \mathbf{M} to break the spatial inversion symmetry of the system, though this usually requires complex magnetic structures.

Using first-principles density-functional theory calculations guided by group-theoretical analysis, we identify a hitherto unknown polar phase of bulk $A_4B_3O_9$ layered

*Contact author: nicholas.bristowe@durham.ac.uk

Published by the American Physical Society under the terms of the Creative Commons Attribution 4.0 International license. Further distribution of this work must maintain attribution to the author(s) and the published article's title, journal citation, and DOI.

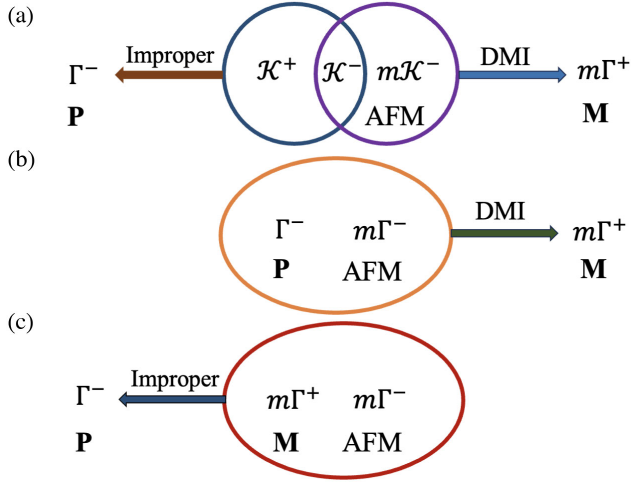


FIG. 1. Trilinear coupling terms in the free energy expansion representing (a) \mathcal{K} -point ME-MF scheme in perovskites involving polarization and magnetization [17], where \mathcal{K} denotes a general zone-boundary point. $m\mathcal{K}^-$ is the irrep associated with AFM ordering, whereas \mathcal{K}^- and \mathcal{K}^+ are the irreps representing nonpolar and nonmagnetic order parameters. (b) Γ -point coupling scheme allowing for the reversal of \mathbf{M} with \mathbf{P} in systems with larger unit cells where AFM order parameters transform as $m\Gamma^-$ irreps. (c) The same Γ -point ME-MF scheme in type-II MFs where the AFM mode couples with \mathbf{M} to induce improper ferroelectricity.

oxides (A : rare-earth and/or alkali-earth cations; B : Co, Ni, Fe) where an applied electric field can switch the magnetization between 180° symmetry equivalent states through the Γ -point ME-MF scheme shown in Fig. 1(b). Full computational details are given in Supplemental Material (SM) [22]. Previous experimental studies on these layered oxides demonstrated long-range AFM ordering of the spins above RT [48,49], indicating the possibility of RT electric field switching of magnetization in $A_4B_3O_9$ layered oxides, which is further supported by our calculations of magnetic exchange interaction parameters. We explain the design principles to stabilize the polar phase with nontrivial ME effect starting from an otherwise nonpolar structure without net magnetization, in the hope of inspiring future experimental work.

Results—Figure 2 shows the crystal structure of the $A_4B_3O_9$ layered oxides that contains slabs of (oxygen-deficient) perovskite-type ABO_3 triple layers translated relative to each other in the basal plane, and separated by rocksalt-type AO layers [49,50], similar to the $n = 3$ Ruddlesden-Popper phases [51]. A sites are occupied by rare-earth and/or alkali-earth elements while the B sites are occupied by transition metal ions. Oxygen vacancies are formed at the central perovskite layer in each block in an ordered manner giving rise to planes of BO_6 octahedra and BO_4 tetrahedra alternating along the out-of-plane direction reminiscent of those in the brownmillerite (BM) phases [52].

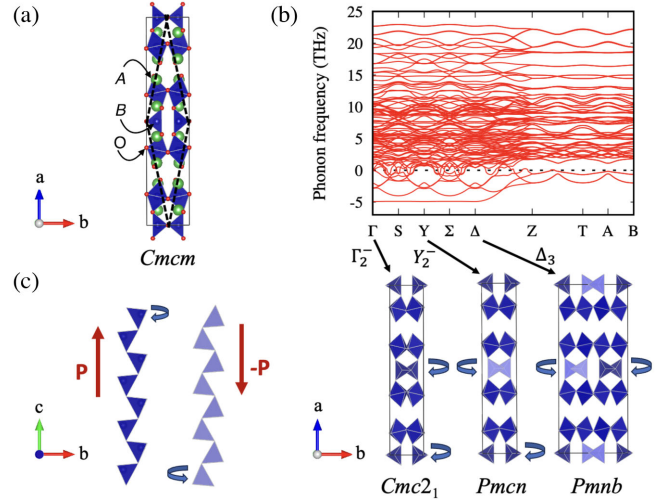


FIG. 2. (a) Crystal structure of the high-symmetry $Cmcm$ phase of the $A_4B_3O_9$ layered oxides consisting of planes of BO_6 octahedra and BO_4 tetrahedra alternating along the out-of-plane direction. Conventional and primitive unit cells are shown by solid and dashed lines, respectively. (b) Phonon spectrum calculated (in the primitive basis) for the $Cmcm$ structure of $Nd_4Co_3O_9$ as a representative of the $A_4B_3O_9$ layered oxides. The phonon dispersion shows a number of instabilities at the zone center and zone-boundary points, which when condensed, result in a variety of structural variants arising from the cooperative rotations of the tetrahedral units. (c) In-plane view of the right- and left-handed tetrahedral chains with opposite polarizations.

$A_4B_3O_9$ layered oxides appear relatively understudied in literature compared to other oxygen-deficient layered compounds like BMs [53–56] and Grenier phases [57–60]. The parent phase of these layered oxides has $Cmcm$ symmetry (no. 63), which contains no rotations of the tetrahedra but allows for tilting of the BO_6 octahedra, as shown in Fig. 2(a). The parent $Cmcm$ structure can also be described as a disordered phase with no long-range ordering of the tetrahedra. Previous experiments on $LnSr_3Fe_3O_9$ (Ln : La, Pr, Nd) show that these layered oxides crystallize into an average structure of $Cmcm$ symmetry without any signature of long-range ordering of the tetrahedral chains [50,61–63]. However, the tetrahedra in these layered compounds can order by rotating about the out-of-plane axis in clockwise and anticlockwise directions leading to the formation of right- and left-handed apex-linked 1D tetrahedral chains with distinct chiralities, analogous to the BMs and Grenier structures. Since the tetrahedra are corner-connected, rotation about the out-of-plane direction is cooperative, i.e., rotation of one tetrahedron (e.g., clockwise) about the out-of-plane direction causes the nearest corner-connected in-plane tetrahedra to rotate in the opposite direction (e.g., anticlockwise).

Depending on the relative ordering of the tetrahedral chains within the unit cell, it is possible to observe a number of structurally diverse phases [22]. When all the tetrahedra rotate in the same direction (either left-handed or

right-handed), the dipole moments arising from the displacement of cations away from the center of each tetrahedron add up, resulting in a polar structure in the $Cmc2_1$ space group (no. 36) that is associated with a polar mode transforming as the $\Gamma_2^-(a)$ irrep of the parent $Cmcm$ phase [see Fig. 2(b)]. Note that in the $Cmc2_1$ structure, electric polarization is in-plane and along the tetrahedral chain direction. On the other hand, if the tetrahedra rotate in opposite senses in successive layers (i.e., intralayer polarization reversing from layer to layer), the dipole moments from each layer cancel out, forming an antipolar structure as depicted in Fig. 2(b). This antipolar structure is related to the $Cmcm$ phase by the $Y_2^-(a)$ irrep that reduces the symmetry from $Cmcm$ to $Pm\bar{c}n$ (no. 62, *bca* setting). A neutron diffraction study by Hansteen *et al.* on $\text{La}_4\text{Co}_3\text{O}_9$ reveals the formation of long range ordering of the CoO_4 tetrahedra along the out-of-plane direction leading to an antipolar phase in the $Pnma$ space group (no. 62) [49].

It is interesting to note that different intralayer and interlayer tetrahedral twisting patterns can further lead to a variety of other distinct phases resulting in superstructures with longer periods, as observed in a local scale in $\text{Ca}_4\text{Fe}_2\text{Mn}_{0.5}\text{Ti}_{0.5}\text{O}_9$ [64]. An example of a superstructure with intralayer switching of tetrahedral rotation patterns described by $Pmnb$ symmetry (no. 62) is shown in Fig. 2(b), which is associated with the $\Delta_3(a, -a)$ irrep of the parent phase. We have identified another novel polar phase with $Pmc2_1$ symmetry that contributes an energy term of the form $Q_{\Delta_3}^2 Q_{\Gamma_2^-} Q_{Y_2^-}$ in the free energy expansion of the high symmetry phase (Sec. S2 F in [22]). This kind of novel ferroelectric phase with a quadratic-bilinear coupling has also been observed in BM oxides [65].

Indeed, our phonon calculations for the paraelectric $Cmcm$ structure of $\text{Ln}_4\text{B}_3\text{O}_9$ (Ln : La, Pr, Nd; B : Co, Ni) and $\text{LaA}'_3\text{Fe}_3\text{O}_9$ (A' : Sr, Ca) compounds reveal a number of instabilities at the zone center and zone-boundary points, which when condensed, result in a variety of structural variants arising from the cooperative rotations of the tetrahedral units, as shown in Fig. 2(b). The phonon spectra calculated for the $Cmcm$ phase of all the considered $\text{A}_4\text{B}_3\text{O}_9$ systems show qualitatively similar features with a strongly unstable flat phonon branch along the $\Gamma - \text{S} - \Sigma - \text{Y} - \Delta$ direction in the Brillouin zone related to the tetrahedral chain ordering distortions. Presence of a flat phonon band indicates that the different structural variants derived from these instabilities will be close in energy (at the harmonic level, at least).

Starting with the optimized structures, we compute the energy of the nonpolar $Cmcm$ phase relative to the polar $Cmc2_1$ phase (ΔE_{NP}) across three sets of compounds containing different B -site cations (B : Co, Ni, and Fe). We find that all the considered materials are insulating with a band gap in the range of 1.2 to 2.4 eV [22]. In each series, inclusion of smaller A -site cations is found to increase the

TABLE I. Energetics and band gaps of the considered $\text{A}_4\text{B}_3\text{O}_9$ layered oxides. Here, ΔE_{NP} is the energy of the nonpolar $Cmcm$ phase relative to the polar $Cmc2_1$ phase. ΔE_{PA} and $Q_{\Gamma_2^-}$ denote the relative energy of the polar $Cmc2_1$ phase with respect to the antipolar $Pm\bar{c}n$ phase and the amplitude of the polar mode, respectively. Band gaps are determined for the lowest energy phases, while $Q_{\Gamma_2^-}$ is calculated for the relaxed $Cmc2_1$ structure of each compound.

| B -site element | Layered oxide | ΔE_{NP} (eV/f.u.) | ΔE_{PA} (meV/f.u.) | $Q_{\Gamma_2^-}$ (Å) | Band gap (eV) |
|-------------------|--------------------------------------|----------------------------------|-----------------------------------|----------------------|---------------|
| Co | $\text{La}_4\text{Co}_3\text{O}_9$ | 0.63 | 0.42 | 1.67 | 2.0 |
| | $\text{Pr}_4\text{Co}_3\text{O}_9$ | 1.09 | 0.11 | 1.72 | 1.9 |
| | $\text{Nd}_4\text{Co}_3\text{O}_9$ | 1.27 | -3.21 | 2.22 | 2.4 |
| Ni | $\text{La}_4\text{Ni}_3\text{O}_9$ | 0.55 | -0.15 | 1.60 | 1.3 |
| | $\text{Pr}_4\text{Ni}_3\text{O}_9$ | 0.73 | -0.32 | 1.65 | 1.2 |
| | $\text{Nd}_4\text{Ni}_3\text{O}_9$ | 0.76 | -0.71 | 1.68 | 1.2 |
| Fe | $\text{LaSr}_3\text{Fe}_3\text{O}_9$ | 0.44 | 0.003 | 1.70 | 1.9 |
| | $\text{LaCa}_3\text{Fe}_3\text{O}_9$ | 0.74 | -9.10 | 1.75 | 1.7 |

degree of tetrahedral rotations leading to higher stability of the low-symmetry phases as shown in Table I.

In Table I, we tabulate the energy of the polar $Cmc2_1$ phase relative to the antipolar $Pm\bar{c}n$ phase (ΔE_{PA}) for the considered layered compounds. The antipolar phase is the ground state (g.s.) for $\text{La}_4\text{Co}_3\text{O}_9$ in agreement with earlier experimental results [49]. However, as we decrease the A -cation size from La^{3+} to Nd^{3+} , the antipolar phase becomes metastable and the g.s. acquires finite polarization with $Cmc2_1$ symmetry. A similar trend in ΔE_{PA} is observed in the Ni and Fe series. Furthermore, the amplitude of the polar mode (see Sec. S2 D in [22] for the definition) computed for the fully relaxed $Cmc2_1$ structure of each compound shows that inclusion of smaller A -site cations increases the polar distortion. Note that this trend in ΔE_{PA} is opposite in BMs where larger tetrahedral chain rotations favor the antipolar phase [66]. In the case of $\text{LaSr}_3\text{Fe}_3\text{O}_9$, ΔE_{NP} is smaller and the polar and antipolar phases have almost identical energies ($\Delta E_{\text{PA}} \sim 0.003$ meV/f.u.), implying that there might not be any long range ordering of the tetrahedral chains [67], consistent with the previous experimental observation of an average $Cmcm$ structure [61,62].

We next check the stability of the polar $Cmc2_1$ structure of the compounds with negative ΔE_{PA} against the formation of superstructures with longer periods of tetrahedral twisting patterns [22]. Focusing on the Co series (due to the challenges of modeling A -cation disorder with density-functional theory in the Fe series, and with the Ni series not yet synthesized), we find that polar $Cmc2_1$ phase is the g.s. of $\text{Nd}_4\text{Co}_3\text{O}_9$. Dynamical stability of the $Cmc2_1$ structure of $\text{Nd}_4\text{Co}_3\text{O}_9$ is shown in Sec. S2 F of SM [22].

$\text{A}_4\text{B}_3\text{O}_9$ compounds are shown to possess above RT magnetic order on the transition metal lattice in earlier experiments [48–50,61]. Previous neutron diffraction

studies on $\text{LnSr}_3\text{Fe}_3\text{O}_9$ (Ln : La, Pr, Nd) [50,61] and $\text{La}_4\text{Co}_3\text{O}_9$ [49] have also characterized the g.s. magnetic structures of these materials where the spins are found to order antiferromagnetically above RT along the tetrahedral chain direction. Considering four collinear spin configurations of the B -site cations, namely, ferromagnetic and A-, C-, and G-type AFM spin arrangements, we first confirm the G-AFM structure as the g.s. for the Co-series compounds as observed in earlier experiments [49]. Noncollinear magnetic calculations including spin-orbit coupling further reveal that all the systems have magnetic easy axis along the tetrahedral chain direction, i.e., in the plane along the [001] direction in agreement with previous experimental observations [49,61]. Details of the g.s. crystal structures and magnetic configurations are given in SM [22].

Interestingly, we find that in the $Cmc2_1$ phase, the polar mode induces a net magnetization perpendicular to the tetrahedral chain direction (i.e., along [010]) via a canting of the antiferromagnetically ordered (C- and G-AFM) collinear spins of the B -site cations along the chain direction (i.e., along [001]), which is otherwise absent in the paraelectric $Cmcm$ phase. Both C- and G-AFM spin configurations in the $Cmc2_1$ structure correspond to the magnetic space group $Cm'c2'_1$ (magnetic point group $m'm2'$), which is related to the high symmetry $Cmcm$ space group by a polar distortion transforming as the $\Gamma_2^-(a)$ irrep and two magnetic distortions transforming as $m\Gamma_3^-(a)$ and $m\Gamma_4^+(a)$ irreps. The $m\Gamma_3^-$ irrep is associated with the primary AFM magnetic ordering, whereas the $m\Gamma_4^+$ irrep represents the secondary wFM mode. Group-theoretical analysis reveals that these three modes couple in an ‘‘improper’’ manner, contributing a trilinear energy term of the form

$$\mathcal{F} = \gamma Q_{\Gamma_2^-} Q_{m\Gamma_4^+} Q_{m\Gamma_3^-}$$

in the free energy expansion of the parent phase, where γ is the expansion coefficient.

As a consequence of this Γ -point coupling, reversal of \mathbf{P} via an electric field would necessarily require reversal of just one of the two magnetic modes. We have investigated this point explicitly via first-principles simulations showing that, upon reversal of the polar distortion, the spins immediately evolve toward a configuration in which the wFM mode switches while the G-AFM order remains the same (see Sec. S2 I in Ref. [22]). Hence we expect 180° reversal of \mathbf{M} with an applied electric field.

Figure 3(a) shows the polarization double well in $\text{Nd}_4\text{Co}_3\text{O}_9$ calculated for the g.s. G-AFM magnetic configuration in the polar $Cmc2_1$ phase with polarization along [001]. Here, we plot the relative energy of the $Cmc2_1$ structure (ΔE) as a function of the polar mode amplitude ($Q_{\Gamma_2^-}$). As seen, ΔE is maximum for the $Cmcm$ phase that corresponds to $P = M = 0$. As we increase $Q_{\Gamma_2^-}$, ΔE

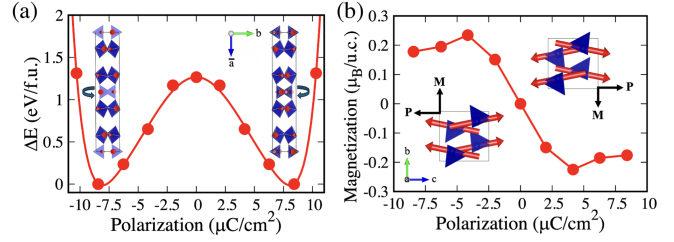


FIG. 3. (a) Polarization switching path in $\text{Nd}_4\text{Co}_3\text{O}_9$ calculated for the polar $Cmc2_1$ phase with G-AFM magnetic configuration. As seen, the sense of rotations of the tetrahedra is flipped as we go from the $+\mathbf{P}$ states to the $-\mathbf{P}$ states. (b) Calculated net magnetization as a function of the polar mode amplitude demonstrating the reversal of magnetization with the reversal of the electric polarization. Spin moments are denoted by red arrows. Note that only the magnetic moments on the tetrahedral sites are shown for clarity.

decreases on both sides, reaching a minimum at the relaxed value of $Q_{\Gamma_2^-}$, and corresponds to $P^0 \sim \pm 8.41 \mu\text{C}/\text{cm}^2$, which is about 2 to 4 times larger than the electric polarization in BMs [55,56,65]. Figure 3(b) shows the resulting net magnetization for the different amplitudes of the polar mode. For small P , the magnetization varies linearly with $Q_{\Gamma_2^-}$, which is consistent with the Γ -point scheme shown in Fig. 1(b), and reaches a value of $M^0 \sim \pm 0.18 \mu_B$ per unit cell for the relaxed value of $Q_{\Gamma_2^-}$. Interestingly, the spin canting angles are flipped as we reverse the electric polarization resulting in opposite net magnetization $-\mathbf{M}$ and $+\mathbf{M}$ in the $+\mathbf{P}$ and $-\mathbf{P}$ states, respectively, demonstrating the switching of magnetization via the reversal of the polar mode. Our first-principles calculations thus predict $\text{Nd}_4\text{Co}_3\text{O}_9$ as an ideal candidate for observing the electric field switching of magnetization.

Finally, to investigate the possibility of RT magnetization switching in $\text{Nd}_4\text{Co}_3\text{O}_9$, we calculate the magnetic exchange parameters (J 's) of $\text{Nd}_4\text{Co}_3\text{O}_9$ and compare them with the J 's of $\text{La}_4\text{Co}_3\text{O}_9$, where RT long range magnetic order has been observed experimentally [48,49]. We find that the calculated J 's for the $Pm\bar{c}n$ structure of $\text{La}_4\text{Co}_3\text{O}_9$ are almost identical to those computed for the g.s. $Cmc2_1$ structure of $\text{Nd}_4\text{Co}_3\text{O}_9$ (Sec. S2 J in [22]), indicating that $\text{Nd}_4\text{Co}_3\text{O}_9$ is also likely to exhibit long range magnetic ordering at RT.

Discussion and conclusions—We have proposed a novel Γ -point ME-MF scheme that allows for the reversal of DMI-induced magnetization with an external electric field and has rarely been observed [7,19] to the best of our knowledge.

Our first-principles calculations reveal a variety of previously unknown structurally distinct phases of the $A_4B_3O_9$ oxides arising from the cooperative rotations of the tetrahedral units. In particular, a polar structure with $Cmc2_1$ symmetry has been identified that allows for a 180° reversal of magnetization by an electric field switching of

the polar mode through the Γ -point ME-MF scheme. We find that smaller A -site cations can induce a larger polar distortion stabilizing the polar $Cmc2_1$ structure with net magnetization.

The calculated values of ΔE_{NP} , which generally measures the upper bound of the switching barrier [56], are in the range of 0.44 to 1.27 eV per formula unit and of the same order of magnitude calculated for similar geometric ferroelectrics [56,68,69]. Previous experimental evidence of ferroelectric switching in thin films of BMs with similar magnitudes of ΔE_{NP} [69] suggests the possibility of experimental observation of electric field reversal of polarization in $A_4B_3O_9$ layered oxides. However, one should note that while these layered oxides draw similarities with BMs, the BMs have not been found to allow for a 180° ME-MF switching scheme.

From our first-principles calculations, we put forward $Nd_4Co_3O_9$ with G-AFM ordered $Cmc2_1$ g.s. as an ideal candidate to observe the ME-MF switching. Moreover, in analogy with previous experimental observations, we predict RT electric field reversal of magnetization in $Nd_4Co_3O_9$, which indicates the possibility of its practical application in the next generation memory devices. Note that magnetic anisotropy is crucial to a robust switching mechanism and must be optimized in future material design. Because of the similar ionic radii of La^{3+} (1.36 Å, C.N. 12) and Nd^{3+} (1.27 Å, C.N. 12), the Nd analog of $LaSr_3Fe_3O_9$ has been successfully synthesized in previous experiments [50]. Therefore, it is likely that the Nd-substituted analog of $La_4Co_3O_9$ can also be synthesized. Moreover, Olafsen *et al.* have demonstrated the preparation of the oxidized compound $Nd_4Co_3O_{10}$ [70], showing the possibility of synthesizing its reduced derivative.

In summary, we have identified a series of new layered oxides that have all the necessary ingredients for the elusive control of magnetization with an electric field at RT. Apart from important memory applications, these materials show a range of intriguingly subtle magnetic and structural phases, apparently coupled to their layered and vacancy ordered nature. This understanding will likely provide new opportunities within related active fields on Ruddlesden-Popper and BM materials such as memristors [71,72], catalysis [73,74], photoferroics [75,76], and 2D magnetism [77,78].

Acknowledgments—U. D. and N. C. B. acknowledge the Leverhulme Trust for a research project grant (Grant No. RPG-2020-206). This work made use of the facilities of the N8 Centre of Excellence in Computationally Intensive Research (N8 CIR) provided and funded by the N8 research partnership and EPSRC (Grant No. EP/T022167/1). The Centre is coordinated by the Universities of Durham, Manchester, and York. This work also used the ARCHER2 UK National Supercomputing Service [79]

and the Hamilton HPC Service of Durham University. We acknowledge useful discussions with Mark S. Senn.

Data availability—The authors confirm that all relevant data that support the findings of this study are included in the Letter and its Supplemental Material.

- [1] T. Lottermoser, T. Lonkai, U. Amann, D. Hohlwein, J. Ihringer, and M. Fiebig, *Nature (London)* **430**, 541 (2004).
- [2] C. Ederer and N. A. Spaldin, *Phys. Rev. B* **74**, 020401(R) (2006).
- [3] T. Zhao, A. Scholl, F. Zavaliche, K. Lee, M. Barry, A. Doran, M. Cruz, Y. Chu, C. Ederer, N. Spaldin *et al.*, *Nat. Mater.* **5**, 823 (2006).
- [4] M. Fiebig, T. Lottermoser, D. Meier, and M. Trassin, *Nat. Rev. Mater.* **1**, 1 (2016).
- [5] N. A. Spaldin and R. Ramesh, *Nat. Mater.* **18**, 203 (2019).
- [6] A. Fert, R. Ramesh, V. Garcia, F. Casanova, and M. Bibes, *Rev. Mod. Phys.* **96**, 015005 (2024).
- [7] C. J. Fennie, *Phys. Rev. Lett.* **100**, 167203 (2008).
- [8] N. A. Benedek and C. J. Fennie, *Phys. Rev. Lett.* **106**, 107204 (2011).
- [9] Y. Tokunaga, Y. Taguchi, T.-h. Arima, and Y. Tokura, *Nat. Phys.* **8**, 838 (2012).
- [10] Y. S. Chai, S. Kwon, S. H. Chun, I. Kim, B.-G. Jeon, K. H. Kim, and S. Lee, *Nat. Commun.* **5**, 4208 (2014).
- [11] V. Kocsis, T. Nakajima, M. Matsuda, A. Kikkawa, Y. Kaneko, J. Takashima, K. Kakurai, T.-h. Arima, F. Kagawa, Y. Tokunaga *et al.*, *Nat. Commun.* **10**, 1247 (2019).
- [12] R. Ramesh and S. Manipatruni, *Proc. R. Soc. A* **477**, 20200942 (2021).
- [13] I. Dzyaloshinsky, *J. Phys. Chem. Solids* **4**, 241 (1958).
- [14] T. Moriya, *Phys. Rev. Lett.* **4**, 228 (1960).
- [15] J. Scott and R. Blinc, *J. Phys. Condens. Matter* **23**, 113202 (2011).
- [16] Y. Yang, J. Íñiguez, A.-J. Mao, and L. Bellaiche, *Phys. Rev. Lett.* **112**, 057202 (2014).
- [17] M. S. Senn and N. C. Bristowe, *Acta Crystallogr. Sect. A* **74**, 308 (2018).
- [18] C. Ederer and N. A. Spaldin, *Phys. Rev. B* **71**, 060401(R) (2005).
- [19] C. Ederer and C. J. Fennie, *J. Phys. Condens. Matter* **20**, 434219 (2008).
- [20] G. R. Clarke, M. R. Lees, C. Ritter, I. da Silva, and M. S. Senn, *Inorg. Chem.* **61**, 10015 (2022).
- [21] U. Dey, M. S. Senn, and N. C. Bristowe, *J. Phys. Condens. Matter* **36**, 095701 (2023).
- [22] See Supplemental Material at <http://link.aps.org/supplemental/10.1103/PhysRevLett.134.136801> for computational details, structural information, and additional electronic and magnetic properties of $A_4B_3O_9$ (A : La, Pr, Nd, Y; B : Co, Ni) and $LaA'_3Fe_3O_9$ (A' : Sr, Ca) layered oxides, which includes Refs. [23–47].
- [23] G. Kresse and J. Furthmüller, *Comput. Mater. Sci.* **6**, 15 (1996).
- [24] J. P. Perdew, A. Ruzsinszky, G. I. Csonka, O. A. Vydrov, G. E. Scuseria, L. A. Constantin, X. Zhou, and K. Burke, *Phys. Rev. Lett.* **100**, 136406 (2008).

- [25] P. E. Blöchl, *Phys. Rev. B* **50**, 17953 (1994).
- [26] S. L. Dudarev, G. A. Botton, S. Y. Savrasov, C. J. Humphreys, and A. P. Sutton, *Phys. Rev. B* **57**, 1505 (1998).
- [27] W. E. Pickett, S. C. Erwin, and E. C. Ethridge, *Phys. Rev. B* **58**, 1201 (1998).
- [28] J. Gebhardt and C. Elsässer, *J. Phys. Condens. Matter* **35**, 205901 (2023).
- [29] S. Uma, T. Vasilchikova, A. Sobolev, G. Raganyan, A. Sethi, H.-J. Koo, M.-H. Whangbo, I. Presniakov, I. Glazkova, A. Vasiliev *et al.*, *Inorg. Chem.* **58**, 11333 (2019).
- [30] B. Almoussawi, V. Duffort, A. M. Arevalo-Lopez, M. Braun, N. Djelal, and H. Kabbour, *Dalton Trans.* **51**, 9522 (2022).
- [31] A. I. Liechtenstein, V. I. Anisimov, and J. Zaanen, *Phys. Rev. B* **52**, R5467 (1995).
- [32] A. Togo and I. Tanaka, *Scr. Mater.* **108**, 1 (2015).
- [33] H. T. Stokes, D. M. Hatch, and B. J. Campbell, ISOTROPY Software Suite, iso.byu.edu.
- [34] R. D. King-Smith and D. Vanderbilt, *Phys. Rev. B* **47**, 1651 (1993).
- [35] D. Vanderbilt and R. D. King-Smith, *Phys. Rev. B* **48**, 4442 (1993).
- [36] K. Momma and F. Izumi, *J. Appl. Crystallogr.* **44**, 1272 (2011).
- [37] K. Yamada, M. Matsuda, Y. Endoh, B. Keimer, R. J. Birgeneau, S. Onodera, J. Mizusaki, T. Matsuura, and G. Shirane, *Phys. Rev. B* **39**, 2336 (1989).
- [38] E. E. McCabe, C. Stock, E. E. Rodriguez, A. S. Wills, J. W. Taylor, and J. S. O. Evans, *Phys. Rev. B* **89**, 100402(R) (2014).
- [39] D. Porter, F. Forte, V. Granata, M. Cannavacciuolo, R. Fittipaldi, M. Cuoco, A. Bombardi, and A. Vecchione, *Sci. Rep.* **12**, 10957 (2022).
- [40] H. T. Stokes, D. M. Hatch, and B. J. Campbell, ISODIS-TORT, ISOTROPY Software Suite, iso.byu.edu.
- [41] B. J. Campbell, H. T. Stokes, D. E. Tanner, and D. M. Hatch, *J. Appl. Crystallogr.* **39**, 607 (2006).
- [42] H.-J. Lee, M. Lee, K. Lee, J. Jo, H. Yang, Y. Kim, S. C. Chae, U. Waghmare, and J. H. Lee, *Science* **369**, 1343 (2020).
- [43] P. Babkevich, D. Prabhakaran, C. D. Frost, and A. Boothroyd, *Phys. Rev. B* **82**, 184425 (2010).
- [44] F. Lloret, M. Julve, J. Cano, R. Ruiz-García, and E. Pardo, *Inorg. Chim. Acta* **361**, 3432 (2008).
- [45] B. Pato-Doldan, L. C. Gómez-Aguirre, A. P. Hansen, J. Mira, S. Castro-García, M. Sánchez-Andújar, M. A. Señaris-Rodríguez, V. Zapf, and J. Singleton, *J. Mater. Chem. C* **4**, 11164 (2016).
- [46] M. Tachiki, *Prog. Theor. Phys.* **23**, 1055 (1960).
- [47] S. Xu, X. Wang, L. Bellaiche, and B. Xu, *Phys. Rev. Lett.* **133**, 046801 (2024).
- [48] R. Rahmani, A. B. G. Trabelsi, F. H. Alkallas, A. Othmani, A. Ziouche, A. Boukhachem, and H. Elhouichet, *Ceram. Int.* **48**, 26432 (2022).
- [49] O. H. Hansteen, H. Fjellvåg, and B. C. Hauback, *J. Mater. Chem.* **8**, 2089 (1998).
- [50] N. Barrier, D. Pelloquin, N. Nguyen, M. Giot, F. Bouere, and B. Raveau, *Chem. Mater.* **17**, 6619 (2005).
- [51] S. Ruddlesden and P. Popper, *Acta Crystallogr.* **11**, 54 (1958).
- [52] A. Colville and S. Geller, *Acta Crystallogr. Sect. B* **27**, 2311 (1971).
- [53] A. Muñoz, C. de la Calle, J. A. Alonso, P. M. Botta, V. Pardo, D. Baldomir, and J. Rivas, *Phys. Rev. B* **78**, 054404 (2008).
- [54] J. Young and J. M. Rondinelli, *Phys. Rev. B* **92**, 174111 (2015).
- [55] H. Tian, L. Bellaiche, and Y. Yang, *Phys. Rev. B* **100**, 220103(R) (2019).
- [56] R. Arras, C. Paillard, and L. Bellaiche, *Phys. Rev. B* **107**, 144107 (2023).
- [57] J.-C. Grenier, J. Darriet, M. Pouchard, and P. Hagenmuller, *Mater. Res. Bull.* **11**, 1219 (1976).
- [58] K. Luo and M. A. Hayward, *J. Solid State Chem.* **198**, 203 (2013).
- [59] Y. Shin and G. Galli, *npj Comput. Mater.* **9**, 218 (2023).
- [60] J. Zhang, S. Shen, D. Puggioni, M. Wang, H. Sha, X. Xu, Y. Lyu, H. Peng, W. Xing, L. N. Walters *et al.*, *Nat. Mater.*, **1**, 912 (2024).
- [61] Ø. S. Fjellvåg, V. Øygarden, M. H. Sørby, and A. O. Sjøstad, *J. Solid State Chem.* **275**, 56 (2019).
- [62] V. Øygarden, H. Fjellvåg, M. H. Sørby, and A. O. Sjøstad, *Inorg. Chem.* **55**, 7630 (2016).
- [63] L. Jantsky, H. Okamoto, A. Demont, and H. Fjellvåg, *Inorg. Chem.* **51**, 9181 (2012).
- [64] H. Krüger, S. Stöber, T. Welberry, R. Withers, and J. Fitz Gerald, *Acta Crystallogr. Sect. B* **67**, 476 (2011).
- [65] H. Tian, X.-Y. Kuang, A.-J. Mao, Y. Yang, H. Xiang, C. Xu, S. O. Sayedaghaee, J. Íñiguez, and L. Bellaiche, *Phys. Rev. Mater.* **2**, 084402 (2018).
- [66] T. G. Parsons, H. D'Hondt, J. Hadermann, and M. A. Hayward, *Chem. Mater.* **21**, 5527 (2009).
- [67] Results in Table I are given only for the electron doped models of $\text{LaA}'_3\text{Fe}_3\text{O}_9$ (A' : Ca, Sr) and as shown in SM [22], relative energies of the polar and antipolar phases of $\text{LaA}'_3\text{Fe}_3\text{O}_9$ vary depending on the cation ordering model considered.
- [68] A. T. Mulder, N. A. Benedek, J. M. Rondinelli, and C. J. Fennie, *Adv. Funct. Mater.* **23**, 4810 (2013).
- [69] K. T. Kang, C. J. Roh, J. Lim, T. Min, J. H. Lee, K. Lee, T. Y. Lee, S. Kang, D. Seol, J. Kim *et al.*, *Adv. Mater.* **31**, 1808104 (2019).
- [70] A. Olafsen, H. Fjellvåg, and B. C. Hauback, *J. Solid State Chem.* **151**, 46 (2000).
- [71] N. Lu, P. Zhang, Q. Zhang, R. Qiao, Q. He, H.-B. Li, Y. Wang, J. Guo, D. Zhang, Z. Duan *et al.*, *Nature (London)* **546**, 124 (2017).
- [72] X. Mou, J. Tang, Y. Lyu, Q. Zhang, S. Yang, F. Xu, W. Liu, M. Xu, Y. Zhou, W. Sun *et al.*, *Sci. Adv.* **7**, eabh0648 (2021).
- [73] R. P. Forslund, W. G. Hardin, X. Rong, A. M. Abakumov, D. Filimonov, C. T. Alexander, J. T. Mefford, H. Iyer, A. M. Kolpak, K. P. Johnston *et al.*, *Nat. Commun.* **9**, 3150 (2018).
- [74] S. Liu, C. Sun, J. Chen, J. Xiao, and J.-L. Luo, *ACS Catal.* **10**, 13437 (2020).
- [75] J.-C. Blancon, J. Even, C. C. Stoumpos, M. G. Kanatzidis, and A. D. Mohite, *Nat. Nanotechnol.* **15**, 969 (2020).

- [76] H. Tsai, W. Nie, J.-C. Blancon, C. C. Stoumpos, R. Asadpour, B. Harutyunyan, A. J. Neukirch, R. Verduzco, J. J. Crochet, S. Tretiak *et al.*, *Nature (London)* **536**, 312 (2016).
- [77] C. Dashwood, A. Walker, M. Kwasigroch, L. Veiga, Q. Faure, J. Vale, D. Porter, P. Manuel, D. Khalyavin, F. Orlandi *et al.*, *Nat. Commun.* **14**, 6197 (2023).
- [78] I. Marković, M. D. Watson, O. J. Clark, F. Mazzola, E. Abarca Morales, C. A. Hooley, H. Rosner, C. M. Polley, T. Balasubramanian, S. Mukherjee *et al.*, *Proc. Natl. Acad. Sci. U.S.A.* **117**, 15524 (2020).
- [79] G. Beckett, J. Beech-Brandt, K. Leach, Z. Payne, A. Simpson, L. Smith, A. Turner, and A. Whiting, ARCHER2 Service Description, Zenodo, [10.5281/zenodo.14507040](https://zenodo.org/record/14507040) (2024).